Politehnica University Timisoara

Abstract

Influence of added hBN on the properties of cermet coatings based on Cr_3C_2-NiCr

Doctoral Thesis

2025

PhD Candidate: Julian Eßler

PhD Supervisor: Prof. Dr. Eng. Ion-Dragoș Uțu

Department: Materials Engineering

Table of Contents

List of abbreviations

BSE	Backscattered electrons
CLSM	Confocal laser scanning microscopy
EDX	Energy-Dispersive X-Ray Spectroscopy
E-Modul	Moduli of elasticity
hBN	Hexagonal boron nitride
HVOF	High-Velocity-Oxygen-Fuel
PFS	Powder flame Spraying
SEM	Scanning electron microscopy

1 Introduction

In the industry, the surfaces of components are often modified or coated to improve wear and corrosion resistance. Among the many options, thermal spraying offers several advantages. In this method, a relatively ductile base material can be used as the coating substrate, which is then coated with a cermet layer, for example, that can achieve a hardness of over 1000 HV [1, 2].

A classic example of cermet coatings (Ceramic & Metallic) is the Cr_3C_2-NiCr coating. These are typically applied using High-Velocity-Oxygen-Fuel (HVOF) spraying. The Cr_3C_2 components ensure wear resistance, and the NiCr content represents the comparatively softer binder matrix. This type of coating has found its origins in the industry as a replacement for the health-hazardous hard chrome coatings [3-5].

Cr_3C_2-NiCr coatings are primarily known for their excellent wear and corrosion resistance, and these factors are influenced by the temperature development due to friction during operation and the associated mechanical wear. Therefore, it is important to continuously improve the properties of such coatings. One way to enhance wear resistance properties can be achieved by adding hexagonal boron nitride (hBN). This can improve the dry-running behavior of these coating systems, which, in turn, also positively affects the emergency running properties. This is due to the two-dimensional structure of hBN. In addition, hBN also possesses excellent oxidation resistance and thermal conductivity.

In this doctoral project, the coating composition will be adjusted by adding hBN to the traditionally used Cr_3C_2-NiCr powder, and the impact on wear properties and thermal conductivity will be investigated. The standard thermally sprayed coatings will be compared with the modified hBN coatings as a reference.

To implement this, a stable powder mixture had to be developed that could be thermally sprayed. Important aspects included the homogeneity of the mixture, the adjustment of the hBN content, the powder feedability and a simple mixing process. The flame spraying and HVOF processes were applied. Flame spraying offers a high deposition rate and minimizes segregation, while HVOF produces particularly dense coatings and embeds the hBN particles well. Wire-based methods were excluded because they are not compatible with hBN. The following Figure 1-1 shows the implementation scheme.

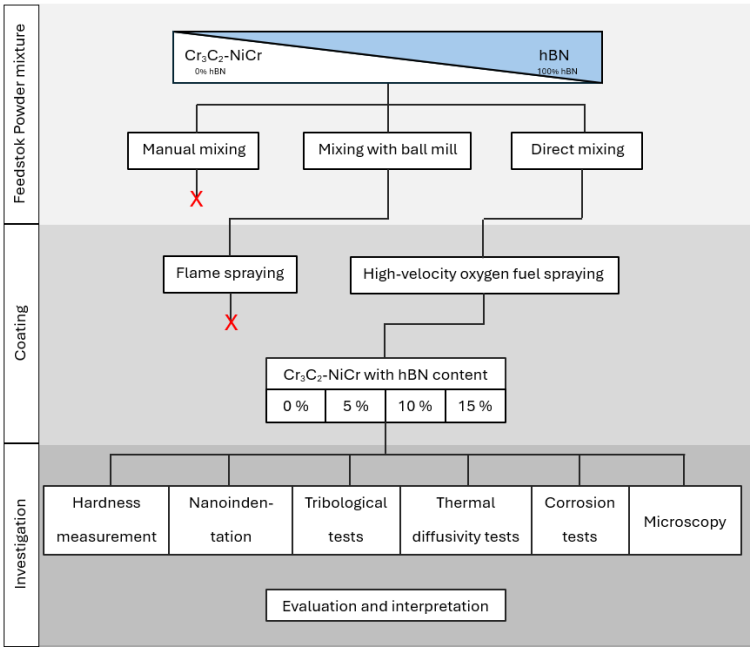

Figure 1-1: Procedure for applying a Cr_3C_2-NiCr/hBN coating

Not all approaches led to successful implementation and were only pursued up to the feasible implementation step (marked with a red "X"). After successfully applying the coating using the HVOF process, the hBN content in the coating was varied. The limits were determined by the maximum hBN content at which the process still ensured sufficient deposition and the coating adhered to the substrate.

2 Current state of science and technology

Thermal spraying:

Thermal spraying is a coating process that enhances components with additional functions, such as improved wear and corrosion protection while preserving the bulk properties of the base material. It is also frequently used for component repair [3, 6].

In this process, a feedstock material is continuously supplied to the spray gun, heated, and applied in a molten state. The substrate is only slightly heated to prevent surface melting and microstructural transformation. Depending on the process and component properties, coating thicknesses can range from 10 µm to several millimeters [7, 8].

Prior to the coating process, cleaning and preparation of the base material are necessary to ensure optimal adhesion. This procedure is specified in DIN EN 13507:2018-10 [8]. Figure 2-1 illustrates the surface preparation process.

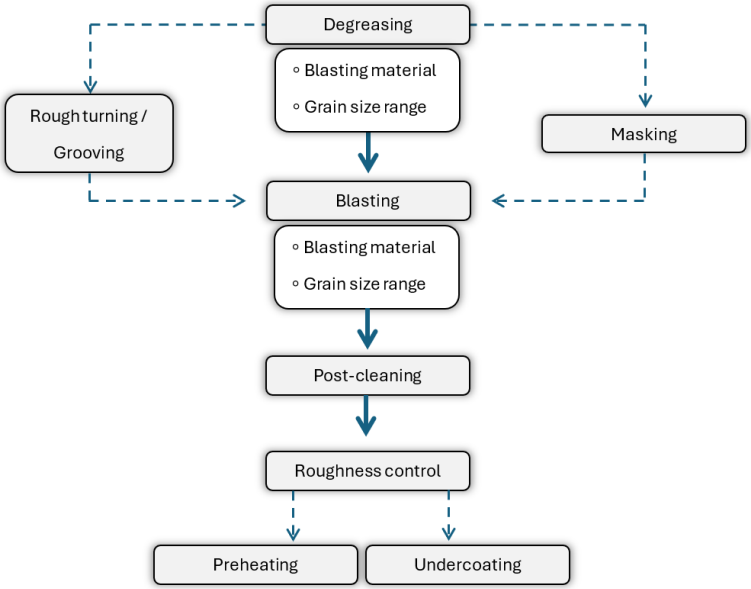

Figure 2-1: General scheme for preparing the surface of substrates for thermal spraying; Angelehnt an das Schema in DIN EN 13507 [8]

Thermal spraying is used for metallic, metal-ceramic, oxide-ceramic, and polymer coatings. Materials are processed in the form of wires, rods, cords, powders, and suspensions [7, 9]. Multilayer systems are often used, where a bonding layer improves the adhesion of the topcoat. One drawback is the remaining porosity without post-treatment. Additionally, only freely accessible surfaces can be coated. Figure 2-2 illustrates the classification of various thermal spraying processes based on their energy sources.

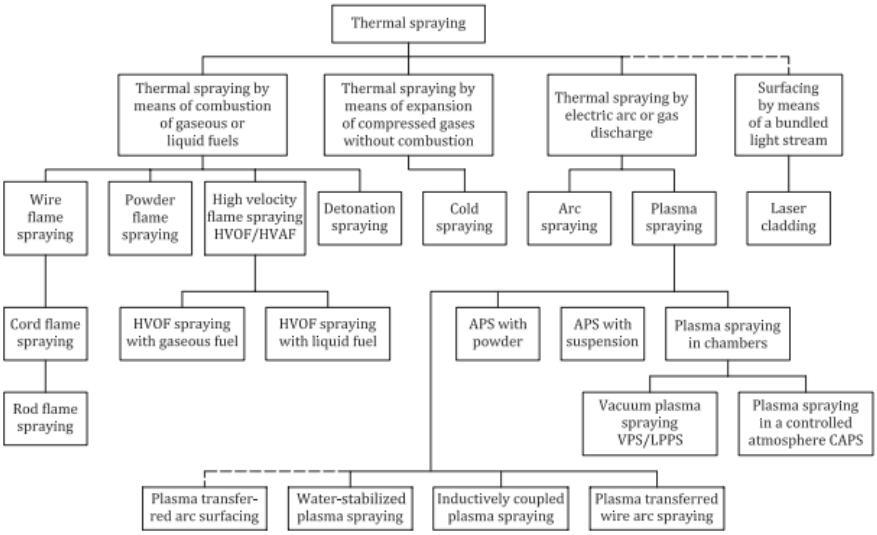

Figure 2-2: Overview of the different thermal spray coating technologies [9]

In flame spraying, the required energy is generated by a fuel gas-oxygen flame. Acetylene, hydrogen, or propane are used as fuel gases, with acetylene being preferred due to its high flame temperature (up to 3160 °C). The feedstock material is available as wire, powder, rod, or cord, leading to different subcategories of flame spraying [10].

In wire flame spraying, the wire is continuously fed into the flame, molten, and sprayed onto the substrate using compressed air. Particle velocities can reach up to 200 m/s. In powder flame spraying (PFS), the material is applied at lower velocities (up to 50 m/s) [9-11].

In high-velocity flame spraying (HVOF/HVAF), the coating material is applied at high speeds (500–700 m/s), resulting in dense coatings with low porosity (<1%) and strong adhesion. The energy source is the combustion of fuel gases (e.g., propane, hydrogen) or kerosene, which enables even denser coatings [9-11].

This process is widely used for wear and corrosion protection coatings, particularly with WC-Co and Cr_3C_2-NiCr. Research focuses on optimizing durability and deposition rates, which typically remain below 80% [12–17]. While wear and corrosion resistance are extensively studied due to their critical role in component longevity, thermal conductivity in thermally sprayed cermet coatings has been rarely investigated.

Cr_3C_2-NiCr coatings exhibit high hardness (approximately 900 HV0.3) and suitable thermal conductivity, reducing cooling requirements. These coatings are considered gas-tight (porosity <1%) and offer better fracture toughness than WC-Co coatings, leading to fewer cracks and significantly higher temperature resistance (service temperature of WC-based coatings up to 450°C, while Cr_3C_2-based coatings can withstand up to 900°C) [18-25].

At elevated temperatures, Cr_3C_2-NiCr coatings are advantageous, as they endure temperatures up to 900°C, whereas WC-based coatings are limited to about 450°C. Additionally, they serve as a safer alternative to WC-Co coatings, as cobalt is hazardous to health. Cr_3C_2-NiCr coatings also provide excellent corrosion and oxidation resistance, even in marine environments. The porosity of the coatings influences corrosion resistance—lower porosity results in improved durability [20, 26-29]. Another key advantage is their frequent use as a replacement for WC-Co coatings, particularly in industries with strict health and safety regulations, such as the food industry [25, 30].

Applications of Cr_3C_2-NiCr coatings are diverse, including brake discs, pump impellers, hydraulic applications, and areas requiring high dimensional accuracy and low fitting wear [19, 25, 31].

The selected additive, hexagonal boron nitride (hBN), is used as a solid lubricant to enhance wear behavior at room temperature and elevated temperatures (400–800°C) [32-34]. However, its role in improving thermal conductivity is less frequently studied. Some research focuses on hBN's resistance to aggressive chemicals [35 36].

The particle size and concentration of hBN significantly influence wear behavior and crack formation in coatings. Higher hBN content reduces coating hardness, allowing lubricating particles to integrate more easily into the matrix. However, excessive particle size or content can lead to cracking and stress inhomogeneity [37].

It has been observed that an increased amount of hBN causes adhesion issues and a reduced deposition rate. A maximum addition of 10 wt.% hBN is considered optimal, as beyond this threshold, embedding hBN into the coating becomes challenging [33, 37-39].

A major challenge in applying hBN-based coatings is its poor wettability with most coating materials, making thermal spraying difficult. High-velocity plasma spraying has been found beneficial in improving coating cohesion [40, 41].

Combining hBN with Cr_3C_2- or WC-based coatings (applied via HVOF) has shown a reduction in the coefficient of friction. However, during wear tests, shear forces often cause hBN particles to detach [32]. Two approaches are being pursued to enhance adhesion and prevent hBN particle separation: optimizing powder preparation or adjusting the coating process.

Ball milling is used to improve the mixing of hBN with metallic powder, enhancing cohesion and resulting in better coating properties [33]. Alternatively, a suspension method can be employed, though this significantly increases equipment setup complexity [34].

Common thermal spraying techniques for hBN coatings include high-velocity plasma spraying, suspension spraying, cold spraying, and high-velocity air-fuel (HVAF) spraying [32, 34, 37-42]. Although HVOF is less frequently used, it provides improved cohesion due to the high kinetic energy of the process [43].

3 Methodology and apparatus

Since previous tests indicated that hBN could separate from Cr_3C_2-NiCr during the coating process, preliminary experiments were conducted to address this issue. Various methods for preparing a processable powder mixture were selected based on feasibility and potential success to enable future large-scale applications. In addition to the HVOF process, the PFS (powder flame spraying) method was also considered, as it introduces the powder directly above the coating gun, which should minimize separation. Although PFS is not typically used for Cr_3C_2-NiCr coatings, it was chosen due to this advantage.

Table 3-1 provides an overview of the mixing methods, outlining their respective advantages and disadvantages, along with the subsequently applied coating technique.

Table 3-1: Overview of powder mixing methods

Powder mixing method	Theoretical (bonding mechanism)	Application method	Pros and cons
Manual mixing	Van der Waal forces	HVOF / PFS	+ Simple mixing process + Fast production volume - Low binding forces
Ball mill	Mechanical clamping	HVOF / PFS	- Complex mixing process - Low production volume + Good binding properties
Manual mixing	surrounding	HVOF	+ Variable adjustment of the composition ○ High but one-time effort for the conversion of the plant technology - Cr_3C_2-NiCr serves as a binder for hBN, therefore the proportion of hBN is more strictly limited

To qualify the mixed powders, they were visually assessed and coated using the selected methods. Subsequently, Scanning electron microscopy (SEM) analyses were conducted to evaluate the coating morphology, and Energy-Dispersive-X-Ray-Spectroscopy (EDX) analysis was used to identify hBN within the coating. After an initial selection, the most promising coating variant was further optimized.

For the prequalified coatings, additional investigations followed, including friction wear tests and corrosion resistance evaluations. Table 3-3 provides an overview of the equipment used and their respective applications.

Table 3-2: Overview of the equipment and methods used

Equipment and Methods	Utilization
Camsizer X2 with the X-Flowmodul	Particle size analysis to adjust the process parameters
PFS system	coating of the base material
Coating system from GTV Verschleißschutz GmbH	coating of the base material
Struers GmbH Cut-off machine	Cutting the samples
Mounting press of company Struers GmbH	embedding the segments
Grinding and polishing machine QPOL 250 A2-ECO of the company ATM Qness GmbH	Grinding and polishing of samples
Confocal laser scanning microscope VK-X260 of the company Keyence Deutschland GmbH	Investigation of crack propagation at the interface and measurement of the wear marks
Scanning electron microscope Sigma 300 VP company Carl Zeiss Microscopy Deutschland GmbH	Examination of the microstructure and composition of the layer
XRD analyser X-Pert of the company Philips GmbH	phase analysis
Universal hardness testing device from KB Prüftechnik GmbH	Hardness measurement HV1 and interface loading using Brinell hardness test
Nano-Indentation / Nano hardness tester NHT3 von der Firma Anton Paar Germany GmbH	Determining the modulus of elasticity (E-modulus)
Pin-on-Disc-device of the company Anton Paar GmbH	sliding wear investigation
Dreielektroden-Zelle and Universalpotentiostaten PGZ 301	Corrosion investigation (current density potential curves)
Laser Flash Apparatus - LFA 467 Hyperflash of the company Netzsch-Gerätebau GmbH	Determination of the thermal diffusivity

As the base material, AISI 316L stainless steel with dimensions of 25 × 10 mm was selected. The surface was degreased and sandblasted with Al_2O_3. The powders used are listed in Table 3-3.

Table 3-3: Data on the feedstock powder materials

Material	***Manufacturer***	***Predetermined particle-size distribution [µm]***	***Density***	***Powder density (bulk density)***
Cr_3C_2-NiCr	*GTV Verschleißschutz GmbH*	*+45/-15*	*-*	*2,7*
hexagonal boron nitride	*Henze Boron Nitride Products AG*	*+12/-8 (averaged size)*	*2,25*	*0,4*

Only coatings from ball-milled powder applied via PFS or through the direct mixing process (HVOF) were successfully deposited. Therefore, the following designation was assigned to the samples listed in Tables 3.4 and 3.5.

Table 3-4: Naming of the HVOF coated samples

Sample name	*relative share of hBN [-]*	*relative share of Cr_3C_2-NiCr [-]*	*hBN feed rate [g/min]*	*Cr_3C_2-NiCr feed rate [%/min]*
0hBN-H	0	100	0	80
5hBN-H	5	95	4	76
10hBN-H	10	90	8	72
15hBN-H	15	85	12	68

Table 3-5: Naming of the PFS-coated samples

Sample name	*hBN content [g]*	*Cr_3C_2-NiCr content [g]*
0hBN-P	0,0	250,0
5hBN-P	12,5	237,5
10hBN-P	25,0	225,0
15hBN-P	37,5	212,5

4 Results and discussion

The particle analysis revealed that 80% of the sieved cermet powder had a particle size ranging from 20 to 43 µm, as indicated by the D10 and D90 values. This aligns with the predefined limits of +45/-15 µm. Only Cr_3C_2-NiCr was analyzed since hBN floated in the dispersing medium. Due to the low mass fraction (≤10%) of hBN in the powder mixture, its influence on process parameters was considered negligible.

Determining particle size distribution is essential for optimizing process parameters, as well as ensuring proper powder flowability. The mixing tube failed to produce a suitable powder mixture for the coating methods because Van der Waals forces were insufficient to bind hBN and Cr_3C_2-NiCr powders together. In the HVOF process, most of the hBN powder remained in the powder hose, leading to an inconsistent mass flow that made coating impossible. In PFS, separation of hBN and Cr_3C_2-NiCr already occurred during the transfer process.

The ball milling method resulted in a significantly more stable powder mixture. The PFS system successfully applied the 0hBN-P, 5hBN-P, and 10hBN-P mixtures. However, at 15% hBN, the

powder's flowability was too low, preventing successful coating (deposition rate <10 µm after three cycles). HVOF application was not possible with these powder mixtures, as the long transport path through the 2.5 m feed hose caused segregation, similar to the issue observed with the mixing tube-prepared powder.

In the HVOF process, a delayed powder feed of hBN (compared to Cr_3C_2-NiCr) was noticeable during the first 15 seconds of the process. After this period, the hBN mass flow stabilized, varying between 0–20% of the total powder feed. However, a mixture ratio of 20/80 hBN/Cr_3C_2-NiCr did not result in a measurable deposition (<30 µm after three cycles) and was therefore not further considered. This was due to hBN's poor adhesion properties and the relatively low amount of Cr_3C_2-NiCr, which prevented sufficient layer formation.

The 15-second delay in hBN feed was attributed to its poor wettability and its platelet-like structure. The powder feeder pushes the powder through the hose to the nozzle, where it enters the gas jet. This process naturally compacts the powder within the hose (bringing the particles closer together). When the process stops, a small amount of hBN continues to flow out of the hose into the active spray jet, creating more space and reducing the compaction within the hose. This effect occurs in every coating process but is significantly more pronounced with hBN powder, leading to startup delays. A prolonged startup time of 30 seconds was established to ensure a stable mass flow of hBN.

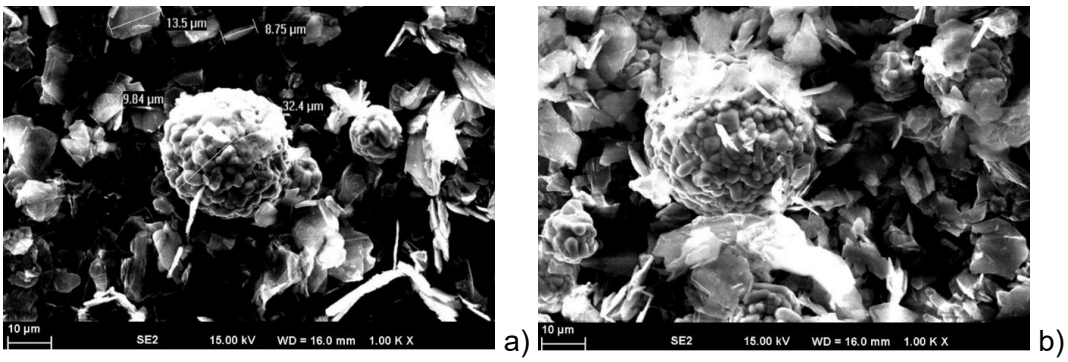

Figure 4-1: Exemplary SEM cross-section in Backscattered electrons (BSE) mode (magnification 1000x) powder mixtures a) 10hBN-P und b) 10hBN-H

Figure 4-1 a) and b) shows that the cermet components in both powders (PFS and HVOF) are clearly coated with hBN, with hBN particles partially adhering in a satellite-like manner to the Cr_3C_2-NiCr particles. The following section will focus on the images of the coated samples.

The sample 10hBN-P shows an unevenly distributed, high porosity, which is atypical for Cr_3C_2-NiCr coatings (see Figure 4-2 a). This results partly from the PFS process, which produces less dense layers than HVOF. Additionally, hBN particles might visually appear as pores or could have been broken out during preparation. Only in the shown sample (Figure 4-2 a) could hBN be detected in the coating. The lamellar structure of hBN is visible (see Figure 4-2 b), but there is no adhesion to the Cr_3C_2-NiCr particles. The hBN particles are surrounded by the cermet components, which also explains the lower deposition rate as the hBN content increases.

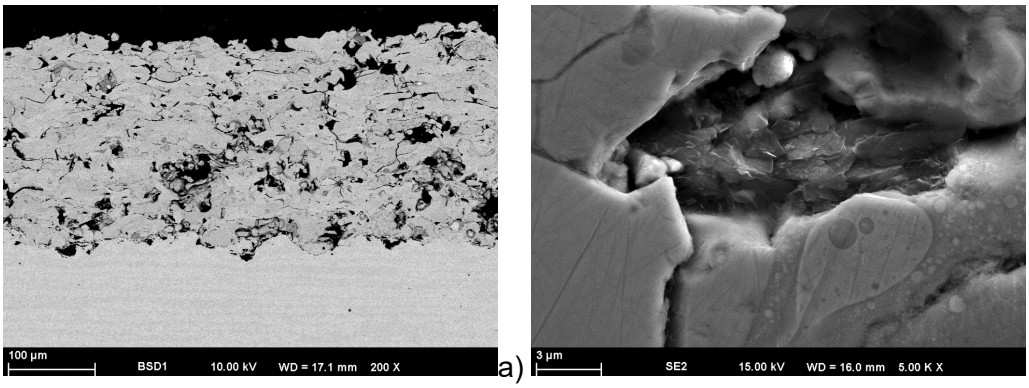

Figure 4-2: Exemplary SEM cross-section in BSE mode of 10hBN-P-coating a) magnification 200x and b) magnification 5000x

The EDX analysis detected Cr, Ni, B, N, and O. Since the temperature during PFS is relatively high compared to HVOF coating, and the particles remain in the flame longer, this coating shows a higher proportion of oxides, which is indicated by the peak at O.

The HVOF-sprayed Cr_3C_2-NiCr coatings exhibit a uniform distribution of components and higher density compared to the PFS coatings (compare Figure 4-2a with Figures 4-3a and b). The deposition rate of the 15hBN-H sample has significantly decreased, while the HVOF coatings with 0-10% hBN show nearly constant coating thicknesses (see Table 4-1).

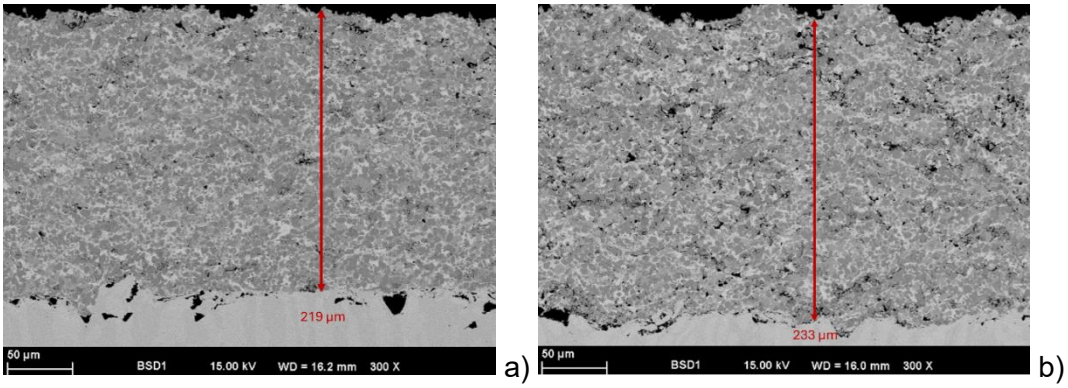

Figure 4-3: Exemplary SEM cross-sections in BSE mode (magnification 300x) with coating thickness markings; a) 0hBN-H and b) 10hBN-H

Table 4-1: Coating thickness of the hBN-H-samples

Sample	***Coating thickness [µm]***
0hbN-H	224 ± 12
5hbN-H	235 ± 15
10hbN-H	226 ± 16
15hbN-H	163 ± 14

As the hBN content increases, porosity also increases (exemplary comparison of Figure 4-3a and b), although a distinction between actual and apparent porosity (due to the hBN content) cannot be made. The 15hBN-H sample shows the highest porosity, while the 0hBN-H sample shows the lowest, confirming that the hBN particles are only enveloped and fixed by the cermet component. Otherwise, hBN would be more distinctly identifiable.

The following Figure 4-4 shows a highly magnified area where an hBN particle has broken out (red marking). Through EDX point analysis (at the yellow-marked spot), traces of B and N were still detected (see Figure 4-5a). The particle breakdown during metallographic preparation

indicates that the cohesion of the coated hBN particles is also limited. This will be discussed in more detail during the tribological and mechanical investigations.

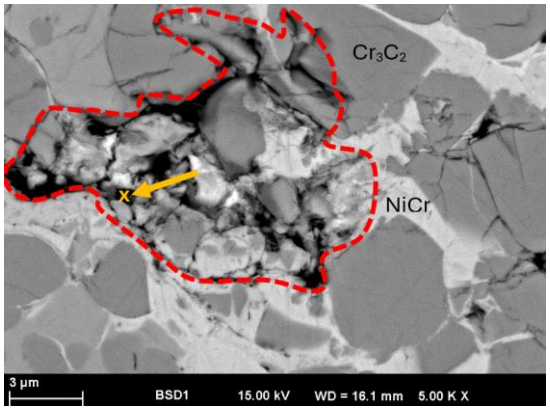

Figure 4-4: Exemplary SEM cross-section in BSE mode (magnification 5000x) of a hole which was created by the pull out of a hBN particle

The XRD spectrum confirms the presence of hBN and correlates with the XRD results. Additionally, the XRD analysis shows that carbides have partially decomposed into $Cr_{23}C_6$ due to the HVOF process.

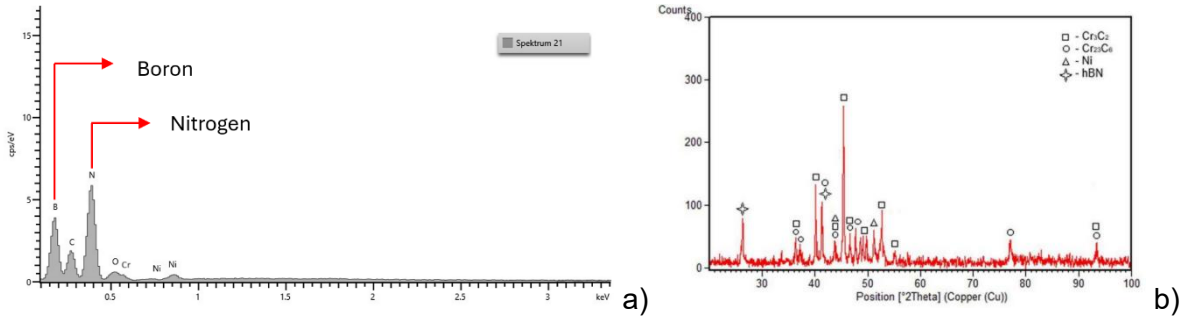

Figure 4-5: a) EDX-Spectrum of the sample 15hBN-H of the yellow marked area of figure 4-4 and b) exemplary XRD-Spectrum of the coating 15hBN-H

The HVOF process produces denser and more homogeneous coatings than the PFS process, which allows hBN to be better embedded, resulting in positive effects on corrosion, wear, and thermal conductivity. Additionally, the direct mixing method eliminates steps in the powder preparation process, improving cost-effectiveness. Since hBN was only detected in the 10hBN-P sample, PFS coatings will not be further investigated.

The following compares the results of hardness and the modulus of elasticity, correlating them with crack tendency.

A comparison of the average hardness of the coatings (see Figure 4-6a) shows that with increasing solid lubricant content, the hardness decreases. This can be explained by the fact that, on the one hand, the hBN particles are much softer than the carbides or the matrix components of the cermets. On the other hand, the lower resistance of the coating bond (compared to the reference) has already been suggested due to the lack of chemical bonding between the hBN and Cr_3C_2-NiCr particles. Since hBN is only fixed by the cermet material, this resistance cannot be developed. Consequently, displacement (including plastic deformation) can occur more easily. The hardness of the coating systems is mainly determined

by the Cr_3C_2-NiCr content. While the hardness loss is small (~2.7%) at 5% hBN and moderate (~12.9%) at 10%, it increases significantly at 15% hBN.

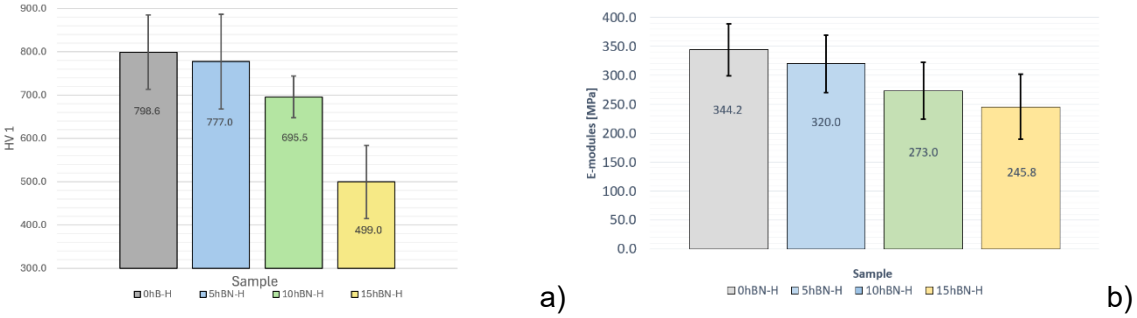

Figure 4-6: Bar chart of a) the HV1-measurements of the samples 0hBN-H to15 hBN-H; b) the E-Module-mean values of the samples 0hBN-H to 15 hBN-H

As the hBN content increases, the E-modulus also decreases (see Figure 4-6b), indicating a reduction in stiffness. However, this does not necessarily improve elasticity, as there is no chemical bonding between the hBN and the cermet (meaning tensile forces cannot be absorbed). A significant impact on crack tendency and wear resistance is expected with an hBN content greater than 10%.

The 5hBN-H and 10hBN-H samples show cracks within the impression, as well as cracks that extend beyond the boundaries. However, these are significantly less pronounced than in the reference layer. In the 0hBN-H sample, a failure of the cohesion and adhesion forces occurs. The crack propagation in the 0hBN-H and 10hBN-H samples is shown for comparison in Figure 4-7 a and b.

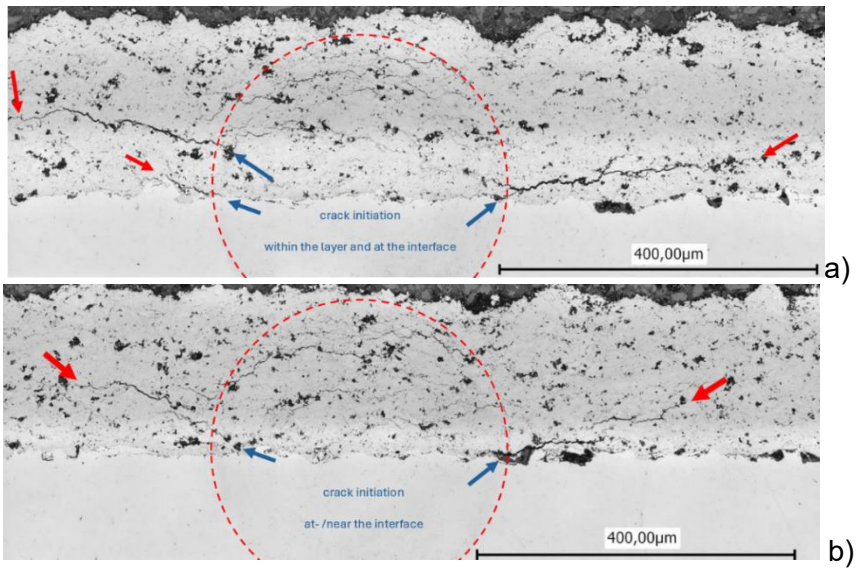

Figure 4-7: Exemplary Confocal laser scanning microscopy-(CLSM)-cross-section (magnification 20x) of the adhesion test with the Brinell method Ø2,5 mm; Load:62,5 kp a) 0hBN-H and b) 10hBN-H (blue arrows mark the crack start and the red arrows mark the crack tip.

Therefore, hBN promotes the elasticity of the coating up to a content of 10%, as it does not initiate additional stresses under load (under compressive stress). This can be explained by the fact that the cermet material—specifically the matrix—can undergo elastic deformation, which is locally damped by the hBN particles. The 10hBN-H sample showed the best resistance to crack propagation. However, at 15hBN-H, significant adhesion and cohesion issues arose, leading to crack networks and delamination.

Crack propagation cannot be assessed by hardness or elasticity alone. Only the combination of both values allows for an accurate assessment, which in turn enables a correlation with crack tendency.

The results of the wear friction tests are presented and discussed in the following.

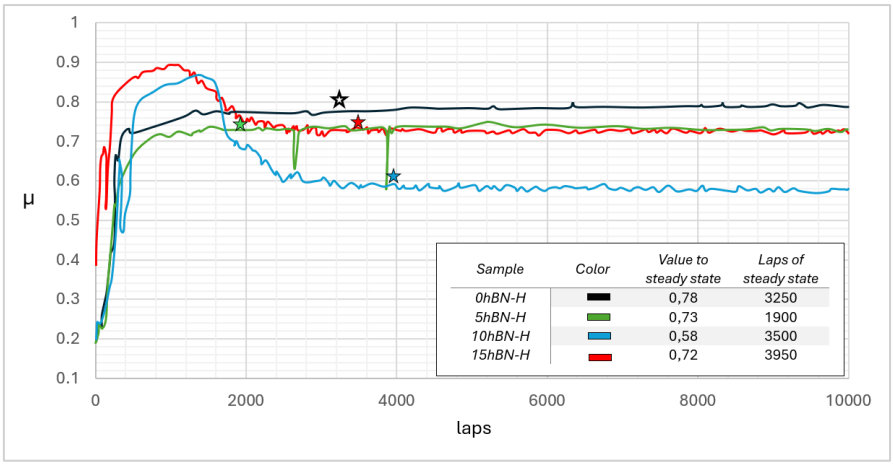

Figure 4-8: Exemplary friction resistance curves from 0% to 15% hBN; Test parameters: 10000 laps; 10 N load; 15 cm/s speed; no lubrication

The results of the coefficient of friction curves shown in Figure 4-8 indicate that up to a content of 10% hBN, the friction resistance decreases. The onset of the steady-state was marked with a star. At a hBN content of 15%, the steady-state friction increases again and approaches the level of the 5hBN-H sample. The 5hBN-H sample shows the shortest run-in distance at 1900 laps. Notably, the 10hBN-H and 15hBN-H samples exhibit a more erratic behavior in the steady-state region compared to the other curves.

No wear volume could be determined for any of the coatings, as no material was removed in depth, only at the surface (see exemplary image in Figure 4-9a). Only wear on the 100Cr6 ball could be identified (Figure 4-9b).

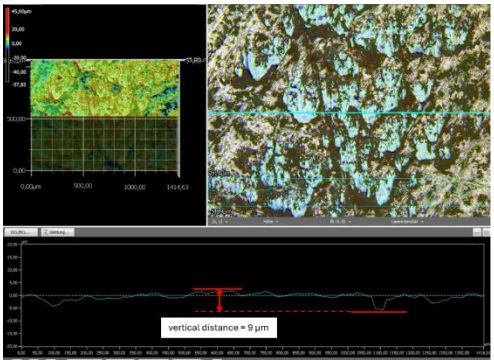

a)

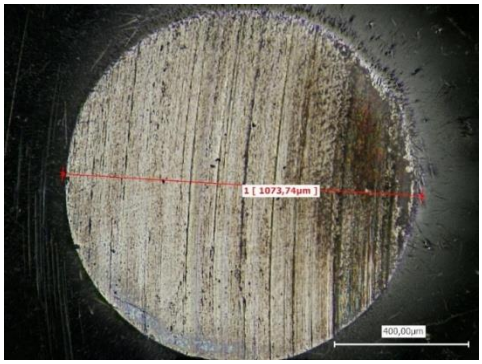

b)

Figure 4-9: a) Exemplary tread depth CLSM-representation x10 of the wear mark of the 15hBN-H sample, b) Presentation of the worn-out surface of the 100Cr6 ball

Initially, the wear ball mainly removes soft matrix components, loosely adhering particles, or hBN. Once the carbides are exposed, the ball slides over the Cr_3C_2 carbides, with the released hBN further supporting the sliding process.

The coatings doped with hBN exhibit improved sliding behavior with lower friction resistances. The longer run-in phase and occasionally higher friction values for 10hBN-H and 15hBN-H are likely due to the initial wear of incompletely embedded hBN particles and surrounding Cr_3C_2-NiCr components. This also explains the previously described erratic behavior (at 10hBN-H and 15hBN-H) in the steady-state region, where smaller chip-offs (< 15 µm) cause fluctuations in the friction curve.

Up to a hBN content of 10%, the particles are stable within the cermet layer and can be gradually released to form a tribological film. Once this threshold is exceeded, the Cr_3C_2-NiCr components can no longer anchor the hBN particles, causing them to break out and adversely

affect the surface topography. As a result, the friction resistance increases, and a more heterogeneous wear landscape is created.

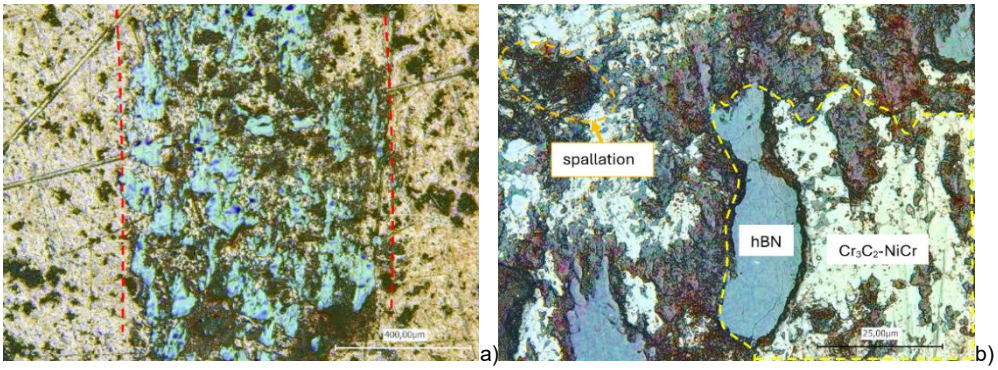

a) b)

Figure 4-10: Exemplary CLSM-recording of sample 10hBN-H; morphology of the tribological lubricant film a) magnification 10x and b) magnification 150x

Figure 4-10a shows an exemplary overview of the wear track for the 10hBN sample. Here, the width of the wear track is bounded by the red dashed lines. The area marked in yellow in Figure 4-10b indicates the zone where a tribological film has formed. The orange marking points to a location where particles have been removed from the coating (spallation). It is also clearly visible that finely distributed hBN is present on the surface. This confirms the previously made statements.

The wear track widths and the wear of the balls (removed diameter) correlate well with each other. It can also be seen that wear decreases up to the 10hBN-H sample and increases again at 15hBN-H. It can be concluded that the addition of hBN results in a reduction of friction resistance by more than 25%.

The results show that the hardness and stiffness of the coating systems interact and must reach a minimum value to ensure sufficient stability for wear loading. For the 10hBN-H coating, these criteria are met. At the same time, the hBN content, with a sufficient cermet layer, positively contributes to the sliding properties. These combined effects result in optimal performance of the 10hBN-H coating in terms of mechanical and tribological properties.

The corrosion tests were conducted in a 3.5% NaCl solution and in a 3.5% NaCl solution with HCl (pH 3.5). The results show that the addition of hBN did not cause any significant change in the corrosion potential or the corrosion current density within a sample series in a given medium. The differences in the curves fall within the measurement deviation for three repetitions. Tables 4-2 and 4-3 illustrate this explanation.

Table 4-2: Corrosion potentials and corrosion current densities of the samples tested in a 3.5% NaCl solution

Sample	*E_{Corr} [mV]*	*I_{Corr} [µA/cm²]*
0hBN-H	*-194*	*0.447*
5hBN-H	*-220*	*0.316*
10hBN-H	*-209*	*0.542*
15hBN-H	*-175*	*0.363*

Table 4-3: Corrosion potentials and corrosion current densities of the samples tested in a 3.5% NaCl +HCl (pH 3.5) solution

Sample	*E_{Corr} [mV]*	*I_{Corr} [µA/cm²]*
0hBN-H	*-276*	*5.848*
5hBN-H	*-282*	*4.416*
10hBN-H	*-289*	*6.457*
15hBN-H	*-280*	*4.217*

To present the tendency of changes in the characteristic features of the curves more clearly, only one of the samples (10hBN) is shown in both media in the following figure. The 10hBN sample is chosen as a representative example of all coating types due to its generally small deviations.

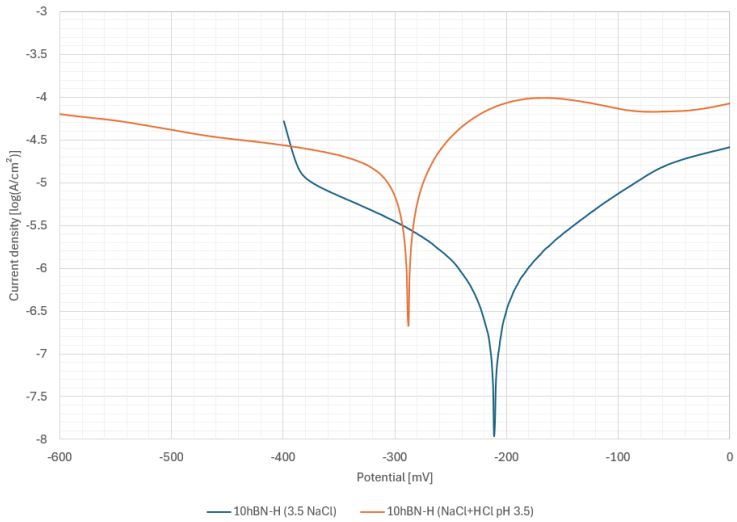

Figure 4-11: Comparison of the semi-logarithmic current density potential curves of the coating 10hBN-H in pure 3.5 % NaCl solution and in 3.5 % NaCl solution with HCl (pH 3.5)

Figure 4-11 shows that the 10hBN-H coating has a corrosion potential of -209 mV and a corrosion current density of 0.542 µA/cm² in a 3.5% NaCl solution. In the medium with HCl, the corrosion current density increases to 6.457 µA/cm², and the potential drops by 80 mV, indicating accelerated corrosion and a less noble character of the material. The base material shows a corrosion potential of -199 mV and a current density of 0.224 µA/cm² in pure NaCl solution. With the pH value lowered to 3.5, the corrosion potential decreases to -338 mV, while the current density increases to 0.317 µA/cm². Compared to the investigated hBN-containing coatings, the potentials in the different media and thus the onset of corrosion show no significant deviations. However, the corrosion current densities in both media are significantly higher – even several times higher at pH 3.5. This is because the matrix, although made of corrosion-resistant NiCr, is present in much smaller quantities compared to a sample of pure AISI 316L material.

The addition of hBN does not result in a significant difference in corrosion resistance, as hBN does not form a chemical bond with the cermets and thus does not form a new phase. The small differences (less than ± 45 mV and less than 1.12 µA/cm²) are merely due to the different topology of the coatings, with some hBN particles being removed after surface preparation. However, these effects do not significantly influence the corrosion behavior. Therefore, all coating types are suitable for use in marine environments (3.5% NaCl) and industrial cleaning processes (pH 3.5) from a corrosion perspective.

The thermal diffusivity was also determined for the sample series 0hBN-H to 15hBN-H. Figure 4-12 lists the thermal diffusivity for the cermet coatings.

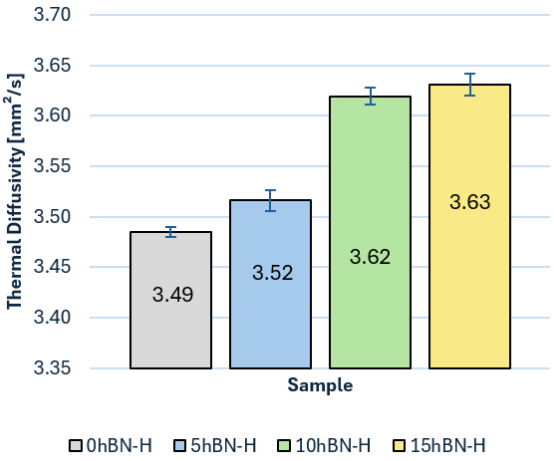

Figure 4-12: Diagram with the mean thermal diffusivity

The diagram shows that the thermal diffusivity is lowest for the reference coating. By adding hBN, it increases. The 15hBN-H sample shows the best value at 3.63 mm²/s (W/m K would also be a commonly used unit). Compared to the reference coating 0hBN-H, the thermal diffusivity improves by up to 4.19%. Again, two effects from adding hBN can be observed. Up to a content of 10%, a significant increase in thermal diffusivity can be identified. Here, the encapsulated particles establish sufficient contact with the cermet components, leading to an increase in thermal diffusivity. As observed in previous studies, a further increase in the hBN content does not significantly improve the investigated properties. The increase in thermal diffusivity from the 10hBN-H sample to 15hBN-H is only 0.3% (see Figure). This is due to the poor adhesion of hBN. If voids exist in the coating due to its structure or because hBN particles have been removed during preparation, heat propagation in the material is hindered, even though it should theoretically increase with a higher hBN content. These voids act as barriers since air has a thermal diffusivity of approximately 0.025 mm²/s, which is relatively low compared to Cr_3C_2-NiCr or hBN. The combination of these effects results in only a minor increase in thermal diffusivity.

Furthermore, it is noteworthy that the standard deviation of the hBN-containing coatings is similar but significantly larger than that of the reference coating. This is due to the direct mixing process used in manufacturing. Process fluctuations can also lead to variations in local hBN concentrations. Additionally, thermal diffusivity depends on the orientation of the particles, which cannot be controlled using this process.

The 15hBN-H sample achieves the best result in terms of thermal diffusivity, while the 10hBN-H sample performs only slightly worse. High thermal diffusivity is important for long component lifespan, and in the case of the 10hBN-H sample, the improvement in thermal diffusivity contributes to better friction and wear performance.

5 General conclusion, further work and personal

Conclusion:

With the HVOF and PFS methods, hBN-doped Cr_3C_2-NiCr coatings were successfully applied. In the PFS process, the powder mixture was prepared using a ball mill, while in the HVOF process, it was done by direct mixing. Both coating methods were prequalified in terms of feasibility and coating quality, which included powder analyses and microstructure comparisons. The results showed that the HVOF method, due to better hBN distribution and a denser coating, was the more suitable variant for further investigations. The results can be summarized as follows:

- If the mass fraction of hBN exceeds 10%, the hardness of the coating system drops drastically. Additionally, the stiffness decreases significantly with more than 5% hBN. This is because the hBN particles do not bond with the Cr_3C_2-NiCr components but are only encapsulated and fixed by them. These two aspects correlate well with crack tendency. Up to a content of 10%, the introduction of hBN is harmless in terms of crack tendency. At a 10% hBN content, a minimal improvement was even observed due to sufficient hardness and reduced stiffness. However, at 15% hBN, complete coating failure (delamination) occurs.
- The best wear resistance properties were observed at 10% hBN, as hBN supported tribological film formation. Higher contents led to worse wear behavior (higher friction resistance, spalls, larger wear track widths).
- At 10% hBN, thermal conductivity increased significantly (up to 4.2%), which partly contributed to improved wear behavior.
- Corrosion tests in 3.5% NaCl solution and in a slightly acidic solution (NaCl + HCl) showed that hBN has no impact on corrosion resistance, as it does not form a chemical bond with Cr_3C_2-NiCr.
- A 10% hBN content offers the greatest potential for improved wear resistance and thermal conductivity, while corrosion resistance remains unchanged.

Outlook:

Further studies in the field of thermally sprayed hBN-Cr_3C_2-NiCr coatings could focus on the following topics:

- The identified optimum of 10% due to the gradual adjustment of the hBN content in 5% steps is limited in its accuracy. It would be beneficial to examine smaller steps of 1% intervals to achieve a more detailed optimization.
- An alternative method for applying hBN-Cr_3C_2-NiCr coatings could be cold gas spraying, due to the comparatively high kinetic energy during the coating process, which represents a promising alternative method. This would offer interesting possibilities to improve the embedding of hBN particles in the cermet coating.
- Variation of the matrix content (increasing the matrix content) could be another approach to better encapsulate the hBN particles and fix them within the coating system.
- Furthermore, it would be of interest to investigate whether the results of this study can be transferred to other cermet materials, such as hBN-doped WC-Co-Cr coatings.

Personal contributions:

Goal of this work was the investigation of the influence of hBN particles on Cr_3C_2-NiCr cermet-based coatings. Initially the knowledge about adhesion, wettability, flowability, friction and wear mechanisms were deepened. Furthermore, the pre-classification enabled a small most

promising choice out of the multitude of different mixing and application approaches. The methods used in this work were considered suitable regarding technical and economic aspects. Beside the technical usability the estimation of the economic efficiency was important due to the intention to transfer the coatings to industrial applications after the completion of the doctoral program.

Due to the bad flowability of hBN the existing coatings systems needed to be modified. These iteration steps lead to the described direct mixing approach where the powder is mixed as late as possible right in the coating stream. Due to the fact that the literature does not give information about the perfect proportion of hBN for an optimum in the mechanical properties, the wear properties and the corrosion properties and its reciprocal conditionality are goal of a corresponding optimisation.

In the literature so far, the heat conductivity was investigated rarely in connection with HVOF coatings, that's why this aspect was from particular importance in this work. Thus, the optimisation was gaining in relevance especially for the industrial use of a Cr_3C_2-NiCr coating with dry-running properties. The particular challenge is the self-lubricating effect while maintaining simultaneously the food contact article conformity for standards and requirements for the food processing industry.

Therefore, a targeted design of the coating was necessary to ensure a high wear resistance, the highest possible heat conductivity as well as an unchanged chemical resistance. These requirements could be fulfilled by the hBN- Cr_3C_2-NiCr composite coating.

Bibliography

[1] B. Song, J. W. Murray, R. G. Wellman, Z. Pala, and T. Hussain, “Dry sliding wear behaviour of HVOF thermal sprayed WC-Co-Cr and WC-CrxCy-Ni coatings,” *Wear*, vol. 442–443, p. 203114, Feb. 2020, doi: 10.1016/j.wear.2019.203114.

[2] E.-S. M. Sherif, M. M. El Rayes, and H. S. Abdo, “WC-Co and WC-Co-Cr Coatings for the Protection of API Pipeline Steel from Corrosion in 4% NaCl Solution,” Coatings, Mar. 2020, p. S. 275. doi: doi: 10.3390/coatings10030275.

[3] Akshay R. Govande, Aayush Chandak, B. Ratna Sunil, Ravikumar Dumpal, “Carbide based thermal spray coatings: A review on performance characteristics and post treatment,” International Journal of Refractory Metals and Hard Materials, 2021. doi: DOI: 10.1016/j.ijrmhm.2021.105772.

[4] M. Jalali Azizpour and M. Tolouei-Rad, “The effect of spraying temperature on the corrosion and wear behavior of HVOF thermal sprayed WC-Co coatings,” *Ceram. Int.*, vol. 45, no. 11, pp. 13934–13941, Aug. 2019, doi: 10.1016/j.ceramint.2019.04.091.

[5] J. A. Picas, M. Punset, E. Rupérez, S. Menargues, E. Martin, and M. T. Baile, “Corrosion mechanism of HVOF thermal sprayed WC-CoCr coatings in acidic chloride media,” *Surf. Coat. Technol.*, vol. 371, pp. 378–388, Aug. 2019, doi: 10.1016/j.surfcoat.2018.10.025.

[6] Santosh Kumar, Rakesh Kumar, “Influence of processing conditions on the properties of thermal sprayed coating: a review,” Surface Engineering, 2021. doi: doi:10.1080/02670844.2021.1967024.

[7] DIN EN ISO 12679, Thermal spraying – Recommendations for thermal spraying, Beuth Verlag, Berlin, Dec. 2015.

[8] DIN EN 13507, Thermal spraying – Pre treatment of surfaces of metallic parts and components for thermal spraying, Beuth Verlag, Berlin, Oct. 2018.

[9] DIN EN ISO 14917, Thermal spraying - Terminology, classification, Beuth Verlag, Berlin, Aug. 2017.

[10] *Prof. Dr. techn. E. Lugscheider (Hrsg.), Handbuch der thermischen Spritztechnik, DVS Verlag, 1. Auflage, 2002*.

[11] *Kirsten Bobzin, Oberflächentechnik für den Maschinenbau, Wiley-VCH Verlag, 1. Auflage 2013, S. 293-316*.

[12] B. Huang, C. Zhang, G. Zhang, and H. Liao, Wear and corrosion resistant performance of thermal-sprayed Fe-based amorphous coatings: A review, *Surf. Coat. Technol.*, vol. 377, p. 124896, Nov. 2019, doi: 10.1016/j.surfcoat.2019.124896.

[13] S. Kumar, A. Handa, V. Chawla, N. K. Grover, and R. Kumar, Performance of thermal-sprayed coatings to combat hot corrosion of coal-fired boiler tube and effect of process parameters and post-coating heat treatment on coating performance: a review, *Surf. Eng.*, vol. 37, no. 7, pp. 833–860, Jul. 2021, doi: 10.1080/02670844.2021.1924506.

[14] W. Tillmann, S. Kuhnt, I. T. Baumann, A. Kalka, E.-C. Becker-Emden, and A. Brinkhoff, “Statistical Comparison of Processing Different Powder Feedstock in an HVOF Thermal Spray Process, *J. Therm. Spray Technol.*, vol. 31, no. 5, pp. 1476–1489, Jun. 2022, doi: 10.1007/s11666-022-01392-2.

[15] J. Oberste-Berghaus, M. Aghasibeig, A. Burgess, P. Khamsepour, C. Moreau, and A. Dolatabadi, Exploring Miniaturized HVOF Systems for the Deposition of Ti-6Al-4V, *J. Therm. Spray Technol.*, vol. 32, no. 2–3, pp. 760–772, Mar. 2023, doi: 10.1007/s11666-023-01531-3.

[16] V. Testa *et al.*, Alternative metallic matrices for WC-based HVOF coatings, *Surf. Coat. Technol.*, vol. 402, p. 126308, Nov. 2020, doi: 10.1016/j.surfcoat.2020.126308.

[17] G. Bolelli *et al.*, Properties of HVOF-sprayed TiC-FeCrAl coatings, *Wear*, vol. 418–419, pp. 36–51, Jan. 2019, doi: 10.1016/j.wear.2018.11.002.

[18] B. He *et al.*, Comparative Study of HVOF Cr3C2–NiCr Coating with Different Bonding Layer on the Interactive Behavior of Fatigue and Corrosion, *Coatings*, vol. 12, no. 3, p. 307, Feb. 2022, doi: 10.3390/coatings12030307.

[19] Shaowu Liu, Hongjian Wu, Shiming Xie, Zexin Yu, Huan Luo, Mohammad Arab Pour Yazdi, Marie-Pierre Planche, Michel Moliere, Hanlin Liao, Effect of stoichiometry conditions on the erosion and sliding wear behaviors of Cr3C2-NiCr coatings deposited by a novel ethanol-fueled HVOF process, Surface and Coatings Technology, 2023

[20] X. Ma and P. Ruggerio, “A Comparative Investigation of Feedstock Materials on Multiple Properties of HVOF-Formed Cr3C2-NiCr Coatings: Size Effects of Powders and Carbides on Sliding Abrasive Wear Behavior,” presented at the ITSC 2024, Milan, Italy, Apr. 2024, pp. 558–569. doi: 10.31399/asm.cp.itsc2024p0558.

[21] Rahul Jude Alroy, M. Kamaraj, G. Sivakumar, HVAF vs oxygenated HVAF spraying: Fundamental understanding to optimize Cr3C2-NiCr coatings for elevated temperature erosion resistant applications, Journal of Materials Processing Technology, 2022

[22] Dervis Ozkan, Structural characteristics and wear, oxidation, hot corrosion behaviors of HVOF sprayed Cr3C2-NiCr hardmetal coatings, Surface and Coatings Technology, 2023,https://doi.org/10.1016/j.surfcoat.2023.129319.

[23] M. S. Priyan, A. Azad, and S. Y. Araffath, “Influence of HVOF parameters on the wear resistance of Cr3C2-NiCr coating,” vol. 4, 2016.

[24] Q. Liu *et al.*, “Microstructural evolution of carbides and its effect on tribological properties of SAPS or HVOF sprayed NiCr–Cr3C2 coatings,” *J. Alloys Compd.*, vol. 803, pp. 730–741, Sep. 2019, doi: 10.1016/j.jallcom.2019.06.291.

[25] Satyapal Mahade, Antonio Mulone, Stefan Björklund, Uta Klement, Shrikant Joshi, Investigating load-dependent wear behavior and degradation mechanisms in Cr3C2–NiCr coatings deposited by HVAF and HVOF, Journal of Materials Research and Technology, 2021,https://doi.org/10.1016/j.jmrt.2021.10.088

[26] K. Wang, S. Hong, Z. Wei, N. Hu, J. Cheng, and Y. Wu, Long-term corrosion behavior of HVOF sprayed Cr3C2–NiCr coatings in sulfide-containing 3.5 wt.% NaCl solution, *J. Mater. Res. Technol.*, vol. 15, pp. 3122–3132, Nov. 2021, doi: 10.1016/j.jmrt.2021.09.131.

[27] Z. Wei, D. Cui, Z. Wei, and S. Hong, HVOF spray of Cr3C2–NiCr coating for enhancing the corrosion resistance of nickel aluminium bronze in 3.5% NaCl solution with different sulphide concentrations, *J. Mater. Res. Technol.*, vol. 23, pp. 869–881, Mar. 2023, doi: 10.1016/j.jmrt.2023.01.050.

[28] L. Fan, X. Li, H. Chen, H. Du, and L. Shi, Corrosion Behavior of Spherical Chromium Carbide Reinforced NiCrBSi Hardmetal Coatings in Sulphuric Acid Solution *Mater. Sci.*, vol. 28, no. 3, pp. 301–308, Aug. 2022, doi: 10.5755/j02.ms.29584.

[29] P. T. Ha *et al.*, A STUDY ON EROSION AND CORROSION BEHAVIOR OF Cr3C2-NiCr CERMET COATINGS, *Vietnam J. Sci. Technol.*, vol. 56, no. 3B, p. 42, Sep. 2018, doi: 10.15625/2525-2518/56/3B/12785.

[30] P. Pereira, L.M. Vilhena, J. Sacramento, A.M.R. Senos, L.F. Malheiros, A. Ramalho, Abrasive wear resistance of WC-based composites, produced with Co or Ni-rich binders, Wear, 2021,mhttps://doi.org/10.1016/j.wear.2021.203924.,”

[31] A. Sharma, A. Vijay, and F. Sadeghi, “Finite element modeling of fretting wear in anisotropic composite coatings: Application to HVOF Cr3C2–NiCr coating,” *Tribol. Int.*, vol. 155, p. 106765, Mar. 2021, doi: 10.1016/j.triboint.2020.106765.

[32] K. Bobzin u. a., „Thermally sprayed coatings for the valve industry“, Mater. Werkst., Bd. 52, Nr. 9, S. 997–1011, Sep. 2021, doi: 10.1002/mawe.202100032.

[33] I. Smid, A. E. Segall, P. Walia, G. Aggarwal, T. J. Eden, und J. K. Potter, „Cold-Sprayed Ni-hBN Self-Lubricating Coatings“, Tribol. Trans., Bd. 55, Nr. 5, S. 599–605, Sep. 2012, doi: 10.1080/10402004.2012.686085.

[34] A. Ganvir u. a., „Novel utilization of liquid feedstock in high velocity air fuel (HVAF) spraying to deposit solid lubricant reinforced wear resistant coatings“, J. Mater. Process. Technol., Bd. 295, S. 117203, Sep. 2021, doi: 10.1016/j.jmatprotec.2021.117203.

[35] Venkata A.S. Kandadai, Jacob B. Petersen, Venkataramana Gadhamshetty, Bharat K. Jasthi, „Synthesis of hexagonal boron nitride nanocoatings for corrosion prevention of iron substrates“, Elsevier, Surface and Coatings Technology, Sep. 2023. doi: https://doi.org/10.1016/j.surfcoat.2023.129736.

[36] Antony Joseph, V. Gautham, K.S. Akshay, V. Sajith, „2D MoS2-hBN hybrid coatings for enhanced corrosion resistance of solid lubricant coatings“, Elsevier, Surface and Coatings Technology, Aug. 2022. doi: https://doi.org/10.1016/j.surfcoat.2022.128612.

[37] Y. Zhao u. a., „Microstructural, mechanical and tribological properties of suspension plasma sprayed YSZ/h-BN composite coating“, J. Eur. Ceram. Soc., Bd. 38, Nr. 13, S. 4512–4522, Okt. 2018, doi: 10.1016/j.jeurceramsoc.2018.06.007.

[38] R. Nikbakht und B. Jodoin, „Thick Cu-hBN Coatings Using Pulsed Gas Dynamic Spray Process: Coating Formation Analysis and Characterization“, J. Therm. Spray Technol., Bd. 31, Nr. 3, S. 609–622, Feb. 2022, doi: 10.1007/s11666-022-01318-y.

[39] Kerem Derelizade, „Thermal spraying of novel composite coating compositions for wear resistance applications“, The University of Nottingham, 2022.

[40] Mou Honglin, Zhao Haichao, Tian Honggang, Ma Guozheng, Liu Ming, Wang Haidou, Xie Fengkuan, Cai Zhihai, „Effects of hBN content and particle size on microstructure, mechanical and tribological properties of NiCr-Cr3C2-hBN coatings“. Elsevier, Surface and Coatings Technology, 29. Februar 2024.

[41] Mou Honglin, Cai Zhihai, Ma Guozheng, Zhou Li, Zhu Xianyong, Liu Ming, Wang Haidou, Xie Fengkuan, Wang Xinyang, „Effects of modification of hBN by nickel plating on coating structure and properties of supersonic plasma spraying NiCr-Cr3C2-hBN@Ni coatings“. Elsevier, Ceramics International, 1. Oktober 2023. [Online]. Verfügbar unter: https://doi.org/10.1016/j.ceramint.2023.07.135

[42] R. K. S. Gautam, U. S. Rao, S. Mishra, und R. Tyagi, „Tribological Behavior of Atmospheric Plasma-Spray-Deposited Ni-Based Composite Coatings at Different Speeds and Temperatures“, J. Therm. Spray Technol., Bd. 29, Nr. 4, S. 756–772, Apr. 2020, doi: 10.1007/s11666-020-01016-7.

[43] M. Oechsner; T. Engler; H. Scheerer; Y. Joung; K. Bobzin; W. Wietheger; M. Knoch; M. Schulz, „Tribological and Corrosion Behavior of HVOF Sprayed Cr3C2-NiCr with Nickel Cladded Graphite and Hexagonal Boron Nitride“, Juni 2021. doi: https://doi.org/10.31399/asm.cp.itsc2021p0732.